Supporting Information

Simonit and Perrings 10.1073/pnas.1112242110

SI Text

S1. Predicted Hydrological Impact of Current Forest Cover. In a baseline exercise we estimated the hydrological impact of current forest cover, using two conversion scenarios. The first conversion scenario involved deforestation of the remaining area of forest cover. Specifically, we assumed that all remaining forest was converted to grassland. The second conversion scenario involved deforestation only of areas where the impact of forest cover on dry-season flows is currently positive (i.e., only the 37% of the existing forest with the soil, slope, and precipitation conditions for a positive effect on total dry-season flow, Fig. 2*A*). The implications of these conversion scenarios for hydrological flows in the Madden and Gatun basins are reported in Table S3 for the three cases: (*a*) current land cover; (*b*) all forest converted to grassland; and (*c*) only forest in areas of appropriate slope, soil type, and precipitation converted to grassland.

Under the first scenario (*b*), conversion of remaining forest to grassland would decrease dry-season flow relative to the current state by 4.7% in the Madden basin, but would increase it by 13.0% in the Gatun basin. The difference in the impact of deforestation in the two basins is explained by the difference in dry-season rainfall. The lower dry-season rainfall in Gatun is associated with greater soil moisture deficiency. In fact, in most of the Gatun basin we found other land covers to dominate forest in the regulation of water flows. Under the second scenario (*c*), conversion of land satisfying the slope, soil, and rainfall conditions associated with positive effects of forest on dry-season flows not surprisingly reduces dry-season water flows in both basins. Specifically, we found that deforestation of beneficial lands reduces dry-season flows by 3.8% in the Gatun basin and by 9% in the Madden basin.

S2. Runoff Estimation. Surface runoff is estimated using the SCS Curve Number method (1). At the core of the approach is a phenomenological model of hydrologic abstraction of storm rainfall (2). The method suits our purpose because it directly addresses the relation between land use and runoff. Although the approach was originally developed to address a single storm event, the method has been used in several long-term hydrologic simulation models (3–5). In our case we use a monthly time step and produce a Curve Number index for each pixel, thus generating a spatially distributed model of excess rainfall. Applying the Curve Number method to monthly input data requires a transformation of the original Soil Conservation Service Curve Number (SCS-CN) equation (6), which includes measures both of runoff depth arising from rainfall and of storage,

$$Q_{it} = \frac{(R_{it} - \lambda S_i)^2}{R_{it} + (1-\lambda)S_i}, R_{it} \geq \lambda S_i, \quad \textbf{[S1]}$$

where Q_{it} is the mean surface runoff depth (millimeters) at the ith spatial unit during month t, R_{it} is mean rainfall depth (millimeters), S_i is a storage index, and λ is a coefficient expressing the initial abstraction assumption (I_i). This assumption implies that runoff will occur only when $R_{it} \geq I_t = \lambda S_i$ and no runoff takes places if $R_{it} < \lambda S_i$. In the original SCS-CN equation initial abstraction is defined by $\lambda = 0.2$. However, the universality of this value has been questioned (2), and several studies have shown that a λ-coefficient locally estimated from field data may improve model fit (3, 7).

The retention or storage parameter varies spatially due to changes in soils, land use, management, and slope. We applied the equation

$$S_i = 25.4\left(\frac{1,000}{CN_i} - 10\right), \quad \textbf{[S2]}$$

where CN_i denotes the Curve Number, a dimensionless index, associated with the ith spatial unit. Theoretically $0 \leq CN \leq 100$; however, empirically the CN index varies from a minimum value of 25, generally for land under forest cover, to a maximum of 100 for areas covered by water. In the typical Curve Number application a CN value is associated with each hydrological unit, generally small subbasins within the main watershed. However, because we are interested in modeling spatially explicit dynamics and water infiltration at the lowest possible scale, we express the CN index at the spatial unit of each pixel. Curve Numbers are normally assigned using established tables relating specific land covers under standard moisture conditions and average 5% slope, to four different soil groups classified according to their hydrological characteristics (1): high infiltration rate (A), moderate infiltration rates (B), low infiltration rates (C), and very low infiltration rates (D).

We enter the caveat that the data on soil characteristics for the region derive from a coarse map (Fig. S6*A*) from a dated soil survey (8). A shift in the classification from one hydrological soil group to another implies a considerable change in estimated runoff with implications for groundwater recharge and low flow response. One concern is that even if the soil map was initially accurate, shifts between hydrological soil groups due to long-term effects of land use change are possible. Deforestation may have a positive impact on dry-season flows only if soil surface characteristics are maintained sufficiently to allow enough rainfall infiltration. In some cases reduced evapotranspiration associated with forest clearance is associated with increased dry-season flow. However, continued exposure of bare soil to intense rainfall, rapid oxidation of soil organic matter, the gradual disappearance of soil faunal activity, and compaction by livestock may all change soil permeability potential. This can lead to a lower dry-season flow despite the reduced evapotranspiration associated with the removal of forest (9).

Forests in tropical environments are expected to differ substantially from similar land cover at more temperate latitudes for which the CN tables have been calibrated. Handbook-defined CN values are most successfully estimated for traditional agricultural watersheds whereas forested watershed estimates are the least successful (10). We estimated the CN index for forest cover from a dataset on runoff and precipitation built for the Candelaria basin within the Panama Canal watershed. The subbasin of 144 km^2 upstream of the Candelaria gauge station has a uniform hydrological soil group (C) and is almost entirely covered (98.5%) by forest. Following ref. 11, an average retention coefficient for each precipitation event (t) can be estimated from observed river flow, $\overline{Q}_t$, and average rainfall, $\overline{R}_t$, for the upstream basin, both expressed in terms of depth:

$$\overline{S}_t = 5\left[\overline{R}_t + 2\overline{Q}_t - \left(4\overline{Q}_t^2 + 5\overline{R}_t\overline{Q}_t\right)^{1/2}\right]. \quad \textbf{[S3]}$$

Thus, any $\overline{R}_t$ and $\overline{Q}_t$ pair yields a solution for $\overline{S}_t$ and, via Eq. **S2**, a CN_t index. Given as many estimated CN_t indexes as observed t

events, it has been shown that the curve number asymptotically approaches a constant value with increasing rainfall (10). It follows that we can solve for the asymptotic curve number (CN_∞), using

$$CN_t(\overline{R}) = CN_\infty + (100 - CN_\infty)e^{-h\overline{R}_t}, \qquad \textbf{[S4]}$$

where h is an empirical constant. The equation may be fitted by a least-squares procedure for CN_∞ and h. The asymptotic constant value is then used in identifying the average CN index for the basin.

We used daily observations [Panama Canal Authority (ACP)] for the Candelaria basin in year 2008. The total direct runoff was obtained by separating the river baseflow from the total hydrographs measured on the Candelaria gauge and considering only daily precipitation events above 10 mm because the relationship between precipitation and runoff becomes evident only above that threshold. The set of estimated CN values associated with each daily event was then used to fit the asymptotic relationship for CN_∞ by a least-squares procedure. The estimated value was $CN_\infty = 75.25$ (P value = 0.000; $R^2 = 0.996$; $n = 111$), which is in line with the $CN = 75$ value estimated for the confining subbasin of the upper Chagres River (12). This has similar land cover conditions to those of the Candelaria basin, with 96.7% of the area covered by primary forest. The estimated value was then recalibrated at $CN = 73.42$ by minimizing the sum of square differences between observed and predicted runoff. Because the average slope of Candelaria basin is 29.29%, the estimated CN index has to be converted to the standard 5% slope condition, using the relationship developed by Sharpley and Williams (13),

$$CN_\alpha = CN + \frac{CN_F - CN}{3}\left(1 - 2e^{-13.86\alpha}\right), \qquad \textbf{[S5]}$$

where CN_α is the slope-adjusted curve number at average percentage of slope α, the latter expressed in decimals; CN is the standard handbook curve number at 5% slope and average moisture conditions; and CN_F is the curve number at 5% slope and wet moisture conditions (i.e., at field capacity), which is determined by a defined empirical relationship (14). Thus, from the estimated $CN = 73.42$ we obtain a standardize value of $CN = 68.57$ at 5% slope and hydrological soil group "C." Applying the curve number aligner set of equations (15), we obtained the CN index values for forest cover on the remaining hydrological soil groups.

The complete set of estimated CN values for natural forest is shown in Table S4. We selected values for other land cover classes in the Panama Canal watershed from the most updated handbook values (16). Values for bare land were taken from CN for fallow conditions in Puerto Rico, residential areas were assumed to compose 65% impervious surface, agricultural CN numbers were taken from row crop values assuming "raw" and "good" management practices, values for grasslands were taken from Puerto Rico, shrubland vegetation was assumed to be equivalent to woods/forest under poor conditions because "rastrojo" land cover is usually associated with secondary forest in recovery or degraded, and values for plantation forests were taken from the CN numbers for wood/forest in "fair" condition.

Applying the coefficients of Table S4, we estimated the CN index for each pixel, using the 2008 land cover map by ACP (Fig. 1) and a hydrological soil group map (Fig. S6*A*) obtained from a soil survey (8). The spatially distributed CN values were then corrected for pixels with slope above the standard 5% value, using a digital elevation model (Fig. S6*B*) and applying the equation proposed by ref. 13. The slope-adjusted CN map is shown in Fig. S6*C*. Following Eqs. **S1** and **S2**, the CN distribution and precipitation maps—the latter obtained from spatial interpolation of long-term averages from 24 ACP meteorological stations—were then used for predicting wet-season runoff, under the initial assumption of $\lambda = 0.2$. The average wet-season monthly precipitation was used in this calculation and the predicted runoff was then multiplied by the number of wet-season months to get the total seasonal runoff.

Predicted runoff during the wet season was compared (Table S1) against long-term (1998–2009) observed values for six subbasins across the watershed. In recent years, land cover has been reasonably constant except for the Ciento subbasin in which there has been a 10% shift from shrubland to grassland between 2003 and 2008. Thus, we compared runoff predictions for this subbasin against a Land Use and Land Cover (LULC) map for 2003, whereas for all of the others we applied the LULC map for 2008. At the initial value $\lambda = 0.2$ the models all overestimated runoff against the observed long-term wet-season values (Table S1). This is an expected result because we applied the original event-based Curve Number approach to predict monthly runoff from monthly average rainfall data. In the SCS-CN equation the relationship of runoff (Q) to rainfall (R) is nonlinear, with Q increasing faster the higher the values of R and the lower the values of CN. Thus, using monthly average rainfall would produce a higher runoff than the estimates obtained by adding up the runoff from individual storm events in the month. Other authors (6) have overcome this by modifying the original equation, using regression analysis and field data. Instead, we scale up the original event-based approach to a monthly time step by recalibrating the value of the initial abstraction coefficient and assuming near-uniform rainfall-runoff proportions at all amounts, durations, and frequencies of precipitation (6). We reestimated λ by minimizing the sum of squared residuals between the observed and the predicted monthly runoffs for all six subbasins, to give $\lambda = 0.7$. The wet-season runoff distribution map after calibration is shown in Fig. S5*A*. After calibration, under-/overestimation of wet seasonal runoff was reduced to within −4.4% and +9.4% (Table S1). The sum of predicted wet-season runoff for all six subbasins was 2,093 million m^3, a +0.3% overprediction if compared with the observed value. Thus, even though the margin of error in predicting total runoff from the basin is minimal, prediction errors vary according to the spatial scale considered.

S3. Groundwater Recharge. Groundwater recharge occurs during the wet season. In the dry season most of the relatively small amount of precipitation infiltrating the soil is lost through evapotranspiration. Groundwater recharge at the ith pixel was estimated as a residual of wet-season precipitation, R_i^w, minus seasonal runoff, Q_i^w, and evapotranspiration, E_i^w, using a water balance approach (i.e., $G_i = R_i^w - Q_i^w - E_i^w$). Net dry-season baseflow was modeled as a function of groundwater recharge, G_i, dry season evapotranspiration, E_i^d, and rainfall infiltration over the same period, $(R_i^d - Q_i^d)$. Water balance implies that potential baseflow in the dry season is equivalent to the groundwater recharge in the wet season. In vegetated areas this is also influenced by evapotranspiration. Vegetation uses the available soil moisture, which we define as the difference between dry-season rainfall and surface runoff. If this is less then the actual evapotranspiration (i.e., $R_i^d - Q_i^d < E_i^d$), groundwater uptake of wet-season recharge will compensate for the dry-season soil moisture deficiency up to the point where uptake does not exceed recharge (i.e., we assume there is no groundwater uptake from adjacent pixels). Thus, the net baseflow contribution from the ith pixel will be lower than the potential baseflow (i.e., $B_i < G_i$) but not negative:

$$B_i = G_i - \left[E_i^d - \left(R_i^d - Q_i^d\right)\right] \geq 0. \qquad \textbf{[S6]}$$

The term in brackets represents the soil moisture deficiency that diminishes the potential dry-season baseflow, forest and grassland being assumed to have the effects described in *SI Text*, section S4. For the ith spatial unit, land cover of type j is denoted Z_{ij}; that with natural forest, Z_{i1}; production forest under teak, Z_{i2}; and grassland, Z_{i3}. If land cover type j is forest or teak, given their relatively lower runoff compared with grassland $(Q_i(Z_{i1}) < Q_i(Z_{i2}) < Q_i(Z_{i3}))$, conversion will have a more strongly negative impact on dry-season flow if condition [**S6**] is binding, such that

$$G_i(Z_{i3}) + Q_i^d(Z_{i3}) > G_i(Z_{i1,\ i2}) - \left[E_i^d(Z_{i1,\ i2}) - (R_i^d - Q_i^d(Z_{i1,\ i2}))\right] + Q_i^d(Z_{i1,\ i2}) = Q_i^d(Z_{i1,\ i2}). \qquad \textbf{[S7]}$$

Otherwise, if condition [**S6**] is not binding or $E_i^d(Z_{i1,\ i2}) < (R_i^d - Q_i^d(Z_{i1,\ i2}))$, it follows that

$$G_i(Z_{i3}) + Q_i^d(Z_{i3}) \gtreqless G_i(Z_{i1,\ i2}) - E_i^d(Z_{i1,\ i2}) + R_i^d. \qquad \textbf{[S8]}$$

From [**S8**] it can be seen that an increase in average dry season rainfall R_i^d increases the probability that forests or teak plantations will have a positive hydrological effect, because—under the SCS Curve Number approach we used for estimating runoff—the variation in $Q_i^d(Z_{i3})$ will always be less than the variation in R_i^d. A decrease in dry-season rainfall has the opposite effect. Rainfall distribution across the watershed therefore determines the hydrological advantage/disadvantage of forest against alternative land covers. In areas with high precipitation (e.g., the Madden basin), forest/plantation is more likely to have a positive impact on dry-season flow than in the areas with low precipitation (e.g., the Gatun basin).

Evapotranspiration (Fig. S5*B*) was estimated as actual evapotranspiration (E_i) from an input map of potential evapotranspiration (P_i) provided by Empresa de Transmisión Eléctrica, SA (ETESA). Following ref. 17, this was obtained by multiplying potential evapotranspiration by a leaf area index coefficient ($k_i = l_i/3$, with $0 \le k_i \le 1$). The leaf area index (l_i) distribution across the basin is derived from the LULC map, assuming $l_i = 3$ for all i under natural forest or teak plantations, $l_i = 2.5$ for shrubland vegetation, and $l_i = 2.3$ for grassland. These values fall within a range of published estimates for specific land covers (18, 19). All other LULC categories, i.e., nonvegetated areas or water, were evaluated at their potential evapotranspiration level (i.e., $k_i = 1$). Given observed precipitation during the wet season, the estimated groundwater recharge map is shown in Fig. S5*C*.

Direct runoff was estimated using the SCS Curve Number approach (1). When it is applied to individual rainfall events, direct runoff estimated using this methodology includes both infiltration excess, representing overland flow, and any subsurface flow that reaches the basin outlet within the time frame of the storm hydrograph. On a monthly time frame the subsurface component, accounted for in the *CN* estimation as direct runoff, would also embed monthly baseflow rather than just representing the sum of event-based quick flows. Because we are calibrating our model on a monthly time frame, using observations on river discharges monthly averages, our direct runoff includes the contribution of monthly precipitation on monthly baseflow. It follows that the wet-season recharge estimated in our model contributes only to dry-season baseflow.

S4. Assumptions on the Hydrological Effects of Different LULCs. We assume that only forest vegetation and teak have the potential to uptake groundwater under soil moisture deficiency conditions and that uptake cannot exceed groundwater recharge at the ith pixel, as specified in Eq. **S6**. In other words, there is no negative contribution to net baseflow by the ith spatial unit. Access to groundwater is limited by advection through capillary rise into the upper soil layers when there is a moisture deficiency. This process is similar to other models describing water movement from the shallow aquifer to the soil profile and ultimately being lost to the atmosphere by evaporation through plant root uptake (20). Under this constraint, if the soil moisture deficiency potentially exceeds recharge and condition [**S6**] is binding, we assume that evapotranspiration is limited and that natural forest and teak plantation would temporarily adjust their water consumption. For other vegetation categories, such as grassland, potential soil moisture deficiency is assumed to limit evapotranspiration directly without generating any groundwater uptake. In other words, grassland does not have any impact on potential dry-season baseflow (G_i) because the deeper wet-season storage is out of the reach of grassland roots. Thus, we assume that its dry-season evapotranspiration is limited by dry-season infiltration alone and the following condition $[E_i^d(Z_{i3}) - (R_i^d - Q_i^d(Z_{i3}))] = 0$ is satisfied. This is consistent with the evidence that most shallow-rooted grasslands dry out during the dry season. For this land cover category and for other vegetated and nonvegetated areas (i.e., shrubland, bare land, and residential areas) we assumed that $B_i = G_i$. It follows that Eq. **1** is then reduced to

$$D_i^d = G_i + Q_i^d. \qquad \textbf{[S9]}$$

Following Eq. **1** and Eq. **S9** and under the condition expressed in Eq. **S6**, we predicted the spatial distribution of hydrological discharge during the dry season (Fig. S5*D*). As for the wet season, our dry-season predictions were tested against the observed long-term values (Table S2). The predicted water volume discharge during the dry season was found to range from −4.0% for the Chico basin to +8.5% for the Ciento basin. Overall, the sum of predicted water flows across the six subbasins was 381.78 million m^3, within −0.6% of the observed value.

S5. Carbon Sequestration by Natural Forest and Teak Plantation. To calculate the carbon storage potential in natural forest, we started with estimates by Heckadon-Moreno et al. (21), who measured aboveground biomass carbon storage in trees from 39 plots scattered across the Panama Canal basin. They reported an average value of 177 tons of carbon per hectare (t C·ha^{-1}) for mature primary forest and 100 t C·ha^{-1} for secondary forest. Using correlations with aboveground biomass, a well-established methodology for estimating carbon stocks in other pools (22), we augmented these estimates by 20% to account for roots (23–26), by 10% to account for litter (23, 25, 27), and by 2% for understory (28). These adjustments yielded values of 234 t C·ha^{-1} and 132 t C·ha^{-1} for primary and secondary forest, respectively. We did not separately account for soil carbon stocks. Preliminary research results from the Agua Salud project site indicate that changes in land cover have little effect on soil carbon stocks, at least over a period of decades. Although soil carbon stocks under mature natural forest (43.0 ± 7.9 t C·ha^{-1}) were found to be significantly higher than the carbon stocks under converted pastures (24.8 ± 2.9 t C·ha^{-1}), there was no accumulation of soil carbon stocks observed over the first 15 y of secondary succession (29).

Plantations are expected to be cut and replanted over a given rotation length. This means that all of the carbon accumulated at the end of the rotation cannot be counted as a carbon benefit because some of it will be emitted during harvesting and processing of the timber. It has been proposed (28) that, in such situations, only the average stock of carbon during the rotation period should be counted as new carbon sequestered. Therefore, in our model we apply an average value of carbon obtained from local studies. For teak plantations, Dale et al. (30) estimate carbon storage following a study by Kraenzel et al. (31) reporting carbon content in above- and belowground biomass at four different locations within the Panama Canal basin based on locally derived allometric regression equations for teak. Considering 25-y rotation periods, they assumed that the average carbon stock would increase over time due to incomplete decomposition of slash and as carbon became sequestered in long-term wood products, whose biomass is reported to be around 30% of the biomass that goes into logs—60% of total biomass (32). Incomplete slash decomposition does not represent an increase in soil carbon pool. In fact teak plantations accumulate little to no soil carbon because the slash does not all decompose during a rotation period, but accumulates over time from one rotation to the next (30), thus being classified as carbon storage from litter accumulation. They found that during the first rotation, the average carbon stock was 82 t C·ha^{-1}, which increased to 113 t C·ha^{-1} at the end of the second rotation and to 116 t C·ha^{-1} at the end of the third rotation. Over how many rotations this pattern of accumulation would continue is unknown and depends on future site preparation (32). We used the Dale et al. (30) estimates for three rotations in our calculations.

S6. Joint Production of Services. We applied a pixel-specific production function yielding four ecosystem services: dry-season water flow, $Y_{i0} = Y_{i0}(D_i^d)$, and three carbon-product bundles corresponding to each land cover type j denoted as Z_{ij}: Z_{i1}, natural forest; Z_{i2}, production forest under teak; and Z_{i3}, grassland. The carbon-product bundles were, for natural forest, $Y_{i1} = Y_{i1}(X_{i1}, 0, 0, Z_{i1})$; for production forest, $Y_{i2} = Y_{i2}(X_{i1}, X_{i2}, 0, Z_{i2})$; and for grassland, $Y_{i3} = Y_{i3}(X_{i1}, 0, X_{i3}, Z_{i3})$; with X_{i1} denoting carbon storage, X_{i2} denoting timber (teak) production, and X_{i3} denoting livestock production.

The spatially disaggregated implicit production function for these services,

$$F_i(Y_{i0}, Y_{ij}, Z_{ij}) = 0, \qquad \textbf{[S10]}$$

defines, for the ith pixel, the output of a set of services comprising dry-season water flows, Y_{i0}; plus the three carbon-product bundles, $Y_{ij},\ \ j = 1, \ldots, 3$; and the land covers that generate each bundle. The choice of land cover on each pixel determines both dry-season flows and the carbon-product bundle supplied by that pixel. Assuming that a single land cover type corresponds to each pixel, the optimal land cover may be obtained from the first-order necessary conditions for maximizing the net benefits yielded by this bundle of services,

$$\pi_i(Y_{i0}, Y_{ij}, Z_{ij}, V, W) = V_0 Y_{i0} + V_j Y_{ij} - W_j Z_{ij}, \qquad \textbf{[S11]}$$

with V_0 and V_j being, respectively, the marginal value of the dry-season water flows and a measure of the marginal value of the carbon-product bundle associated with the jth land cover type and W_j being the marginal cost of the jth land cover type.

The first-order necessary conditions for optimization of Eq. **S11** subject to Eq. **S10** were obtained by setting the partial derivatives of the Lagrangian function

$$L_i = V_0 Y_{i0} + V_j Y_{ij} - W_j Z_{ij} + \mu_i F_i(Y_{i0}, Y_{ij}, Z_{ij}) \qquad \textbf{[S12]}$$

with respect to the choice variables (land covers) equal to zero. The multiplier, μ_i, is a measure of the marginal social value of a small variation in watershed outputs and inputs. These conditions include

$$\begin{aligned} \frac{\partial L}{\partial Y_{i0}} &= V_0 + \mu_i \frac{\partial F}{\partial Y_{i0}} = 0 \\ \frac{\partial L}{\partial Y_{ij}} &= V_j + \mu_i \frac{\partial F}{\partial Y_{ij}} = 0 \\ \frac{\partial L}{\partial Z_{ij}} &= W_j + \mu_i \frac{\partial F}{\partial Z_{ij}} = 0 \\ \frac{\partial L}{\partial \mu_i} &= F(Y_{i0}, Y_{ij}, Z_{ij}) = 0 \end{aligned} \qquad \textbf{[S13]}$$

for all land cover types and associated carbon-product bundles. It follows that for all j

$$\frac{V_0}{V_j} = -\frac{\partial Y_{ij}}{\partial Y_{i0}} = \frac{\partial F/\partial Y_{i0}}{\partial F/\partial Y_{ij}}. \qquad \textbf{[S14]}$$

The rate of transformation between ecosystem services is the rate at which one service has to be given up to obtain the other, measured in Eq. **S14** by $-\partial Y_{ij}/\partial Y_{i0}$. Efficiency in joint production requires that the rate of transformation between any pair of services (the rate at which they are substituted in production) is equal to the ratio between the marginal values of each service. So Eq. **S14** states that the rate of transformation between dry-season water flow and carbon-product bundle associated with land cover j should be equal to the ratio of their marginal values. Eq. **S13** also implies that

$$W_j = V_0 \frac{\partial Y_{i0}}{\partial Z_{ij}}. \qquad \textbf{[S15]}$$

That is, the cost of land cover j should be equal to the value of the marginal product of that land cover type with respect to dry-season water flow. The same condition holds for all other ecosystem services.

The marginal value of dry-season flows depends on dry-season water levels in Gatun Lake and the Canal and is measured in terms of the impact of a unit of flow on the expected transit toll revenue, considering that each lockage uses on average 211,200 m^3 of water (33). One lockage includes both the lifting up of the vessel to the Gatun Lake level and the lowering back to sea level. Because two or more vessels may be included in a chamber for a lockage, lockages and ship transits are not equivalent terms. In 2009 the ACP toll revenue was 1.438 billion US$, with 12,641 total lockages, implying an average revenue of 113,776 US$ per lockage.

The marginal impact of dry-season flow on the number of lockages depends on the factors affecting the volume of water in Gatun Lake: precipitation, temperature, infiltration, evapotranspiration, land use, and land cover in the watershed. Because there is an upper bound to the volume of usable water in the system (4% of annual precipitation is discharged at the Gatun spillway during the rainy season), hydrological flows above a certain level have no impact on water levels. There is also a lower threshold below which the draft in the locks is reduced, as occurred during the 1982–1983 and 1997–1998 El Niño droughts. Below this threshold, declining water levels affect both the number of lockages and toll revenue per lockage, because draft restrictions limit access to the Canal to smaller vessels, and tolls increase with the size of the vessel. Above this threshold additional water flow continues to increase the number of lockages possible, but the marginal impact of flow on the number of possible lockages decreases, falling to zero at the point where additional flow has no effect on water levels (when water levels are at the upper bound).

We estimate the marginal revenue product of dry-season water flows from the Panama Canal watershed via a factor (α) that scales the toll revenue as a function of current water levels at Gatun Lake relative to the draft restriction level and the level at the spillway. Thus, we assume that total toll revenue is a power function of the current water level in Gatun Lake, with the exponent in the power function, α, itself a function of the current water level relative to the draft restriction level and the level at the spillway,

$$\alpha = \left(\frac{U_s - U_t}{U_s}\right)^{\frac{U_t - U_m}{U_t}}, \qquad \textbf{[S16]}$$

where U_s is the spillage level, U_m is the draft restriction level, and U_t is the actual water level at Gatun Lake. This functional form implies that the scaling factor is zero at the spillway, unity at the draft restriction level where the draft of the locks is still at its maximum, and above unity at levels farther below the point at which draft restriction is first implemented. Thus, given the average water use (211,200 m^3) and revenue (113,776 US$) per lockage, the marginal value (V_0) of a cubic meter of water added at water level U_t is

$$V_0 = \alpha \frac{113,776}{211,200}. \qquad \textbf{[S17]}$$

For the spilling level (26.67 m), the draft restriction level (24.84 m), and the long-term average dry-season (January–April) level obtained from daily observations for the period 1995–2009 (26.13 m), the mean marginal value of dry-season water in terms of toll revenues was 0.44 US$$\cdot m^{-3}$. The long-term average dry-season water level reflects water storage in both Madden and Gatun Lakes at the beginning of the dry season, plus the seasonal water evaporation losses net of direct precipitation on the lake surface, and the other water uses (municipal, industrial, and hydroelectric) during the dry season. Note that we do not account for within-season flow dynamics.

The value of sequestered carbon was based on a review of prices in the voluntary market. Carbon prices vary widely among regions and projects and over time. Forestry projects, in particular those involving afforestation/reforestation, are among the highest-priced project types with weighted average prices of 6.8 US$ to 8.2 US$$\cdot t^{-1}$ C across 2006 and 2007 (34). The price for avoided deforestation ranges from 2 US$ to 30 US$ with an average value of 4.80 US$$\cdot t^{-1}$ C (35). Others report that a price for stored carbon of 10 US$$\cdot t^{-1}$ C is more realistic and could increase over the coming decades (36). However, Neef et al. (37) consider that the most reliable price remains that established by the BioCarbon Fund of 4 US$$\cdot t^{-1}$ C. We assumed the value of 1 t of sequestered carbon to be 4 US$, based on the lower average bound value reported in ref. 37.

The value of livestock production was calculated as follows. Current livestock density in the basin is around one animal per hectare of grassland (38), which is in line with the data for the rest of the country. Animals are usually sold at 28–32 mo old, and the average weight of a 2-y-old animal, depending on strain, lies in the range 449 kg (Brahman) to 411 kg (Criollo) (39). In the exercise reported in this paper, we assumed that animals were turned over at 2-y intervals. Live weight prices in Panama in 2009 ranged from 1.00 to 1.32 US$$\cdot kg^{-1}$. Assuming an average price of 1.16 US$$\cdot kg^{-1}$ and an average weight of 430 kg, we calculated mean livestock revenues to be 499 US$$\cdot ha^{-1}$ over 2 y, implying that mean forgone livestock revenue from reforestation was 249 US$$\cdot ha^{-1}\cdot y^{-1}$.

For teak production, we took the average stumpage price of 280 US$$\cdot m^{-3}$ in 2009, as reported for neighboring Costa Rica's timber market (40). Under the Reducing Emissions from Deforestation and Forest Degradation (REDD+) program, timber extraction can be added to carbon storage as complements in production, under sustainable forest management. This implies a periodic yield of wood while maintaining the production potential of the forest. Sustainable timber extraction is based on the growth rate of the timber species based on the mean annual increment, which for teak in Central America has been reported at 10 $m^3\cdot ha^{-1}\cdot y^{-1}$ (41). Thus, we applied a mean (undiscounted) net revenue for teak timber production of 2,800 US$$\cdot ha^{-1}\cdot y^{-1}$. Because we analyze a steady-state solution with fixed rotation age, we do not discount the stream of net revenues. This implies the additional assumption that teak plantations have an equal area in each age class—what is referred to as a "normal" forest. Note that because we do not factor in variations in rainfall, slope, and soil to estimates of biomass yields, the stumpage value is a first approximation only. Using these values in Eq. **S11**, we estimated the extent of the land area for which condition [**S14**] holds, given different bundles of services. The results are reported in Fig. 2.

S7. Sensitivity Analysis. We estimated *CN* values for natural forests, using the hydrograph of a subbasin entirely covered by forest in the upper watershed (*SI Text*, section S2) because there are no values reported for tropical forests in the literature. However, the *CN* values used for other land covers were derived from the literature. We therefore tested the sensitivity of our results to variation in *CN* numbers across the ranges reported in the literature (1, 16). The ranges reported for "woodland", for example, are 55–66 (soil group B), 70–77 (soil group C), and 77–83 (soil group D). For teak forest plantation we used values of 60, 73, and 79, which were the median values within these ranges. For grassland we used a study from Puerto Rico reported in ref. 16 that yielded estimates of 70, 80, and 84, respectively, the ranges reported in the literature being 61–79 (soil group B), 74–86 (soil group C), and 80–89 (soil group D). We tested the sensitivity of our results on dry-season flows to variations of the Curve Number parameters associated with each land cover type. Dry-season flow estimates for the two reforestation scenarios (grassland conversion to natural forest and teak) seem robust to variation in *CN* values (Fig. S2), consistently showing a negative hydrological impact except at parameter values well beyond the range reported in the literature.

Note that parameter variation by 10% (0.9 and 1.1 deflection) can be interpreted as a shift between hydrological soil group categories used to define *CN* values for each land cover type (Table S4). Thus, dry-season flow predictions are as sensitive to the quality of information on soil characteristics as they are to the reference values of the *CN* table.

We also tested the spatial sensitivity of grassland conversion to the hydrological parameters used in the Curve Number approach, given the marginal value associated with different bundles of ecosystem services (Fig. S3). We found higher sensitivity to low *CN* values for both teak and natural forest. Nevertheless, our results referring to the full bundle of ecosystem services (Fig. S3*E.1*) and to water regulation alone (Fig. S3*A.1* and *A.2*) are not affected by variation in *CN* numbers beyond the range reported in the literature. For grasslands, we found variation in *CN* numbers affected both dry-season flow and optimal reforestation. Thus, parameters for grassland should be carefully chosen, possibly following site-specific estimation as in the approach we followed for natural forest (*SI Text*, section S2).

Our estimates of the marginal value of the different ecosystem services are first approximations. They are potentially affected by a number of exogenous trends, and they assume steady-state values for the carbon-product bundles associated with different land cover types. We therefore also tested the sensitivity of the proportion of grassland conversion to variation in the price parameters (Fig. S4). Important sources of uncertainty about the marginal value of ecosystem services include the effect of the Panama Canal expansion on aggregate freshwater use; the effect of current developments in the global market for carbon; and attempts to link carbon, biodiversity conservation, and watershed protection in the REDD+ scheme. In addition, differences in the time it takes for various land cover types to converge on the steady state may affect their relative value. We therefore evaluated the sensitivity of our results on grassland conversion into both natural forest and commercial teak plantation to variation in ecosystem services "prices" relative to our base case: i.e., water at 0.44 US$$\cdot m^{-3}$, carbon at 4 US$$\cdot t^{-1}$ C, the stumpage price of teak at 280 US$$\cdot m^{-3}$, and livestock production at 249 US$$\cdot ha^{-1}$.

We found grassland conversion into natural forest to be highly sensitive to changes in ecosystem service prices (Fig. S4*A*). In our base case, hydrological flow regulation and carbon sequestration services together justify a 59.6% conversion of grassland area in the watershed after accounting for the opportunity cost of forgone livestock production. Because 95.7% of existing grassland, if converted to natural forest, would produce a negative impact on dry-season hydrological flows in the watershed, an increase in water price would increase this externality, thus reducing the percentage of efficient grassland conversion. The opposite happens with a decrease in water price. The effect of water price variation stabilizes at around 10% conversion, mostly localized in the most "hydrologically suitable" lands.

We found reforestation to be more sensitive to changes in the value of land for livestock production, stabilizing at around 5% of grasslands. It is most sensitive to variations in carbon price, the optimal extent of reforestation ranging from 4.7% grassland conversion at 2 US$$\cdot t^{-1}$ C to 97.8% at 6 US$$\cdot t^{-1}$ C. A carbon price above 6.70 US $$\cdot t^{-1}$ C would justify 100% grassland conversion to natural forest.

When we considered grassland conversion to commercial teak plantations, we found much less sensitivity to changes in the marginal value of ecosystem services (Fig. S4*B*). The base case results hold for variations in both carbon prices and livestock production. Timber price variations impact the optimal extent of grassland conversion only below 56 US$$\cdot m^{-3}$. Because commercial plantations are likely to offer few habitat benefits, and because they perform worse than natural forests with respect to both water regulation and carbon sequestration, we might expect the optimal forest structure to involve a greater mix of natural forest and commercial plantations than in our base case. Mixed forest plantations of local species may therefore represent a valid alternative to the monocultural teak forestry even though their stumpage prices are reported to be considerably lower, ranging from 38.8 US$$\cdot m^{-3}$ for *Terminalia amazonia* to 108.6 US$$\cdot m^{-3}$ for *Hyeronima alchorneoides* (42).

Our base case results are also stable in the face of variations in the marginal value of water flow regulation. Only at prices above 1.76 US$$\cdot m^{-3}$ is there a significant effect on optimal grassland conversion. Although we would expect tolls to capture a significant part of the benefit to shipping companies of routing through the Canal, we note that one study reported an average value of water to shipping companies using the Canal up to 1.16 US$$\cdot m^{-3}$ (43). We have also excluded the social benefits of reduced emissions of CO_2, NO_x, and SO_2, which would increase the marginal social value of water regulation above our base case.

We also tested the sensitivity of the percentage of current forest cover yielding positive net benefits from the bundling of two services—hydrological flow regulation and carbon sequestration (Fig. S4*C*). For our base case, 98.4% of existing forest has a positive value for the two aggregated services. We found that our results were not sensitive to variation in the marginal value of water flow regulation. They were, however, sensitive to a decrease in the price of carbon used in the base case: 4 US$$\cdot t^{-1}$ C.

1. USDA Soil Conservaton Service (1972) Estimation of direct runoff from storm rainfall. *National Engineering Handbook* [Soil Conservation Service (SCS), Washington, DC], Sect 4.
2. Ponce VM, Hawkins RH (1996) Runoff curve number: Has it reached maturity? *J Hydrol Eng* 1(1):11–19.
3. Mishra SK, Singh VP (2004) Long-term hydrological simulation based on the Soil Conservation Service curve number. *Hydrol Processes* 18:1291–1313.
4. Pandit A, Gopalakrishnan G (1996) Estimation of annual storm runoff coefficients by continuous simulation. *J Irrig Drain Eng* 122(4):211–220.
5. Williams JR, LaSeur V (1976) Water yield model using SCS curve numbers. *J Hydraul Eng* 102:1241–1253.
6. Ferguson BK (1996) Estimation of direct runoff in the Thornthwaite water balance. *Prof Geogr* 48(3):263–271.
7. Bosznay M (1989) Generalization of SCS curve number method. *J Irrig Drain Eng* 115(1):139–144.
8. Catastro Rural de Tierras Y Aguas de Panamá (1970) *Final Report on the Catastro Rural de Tierras y Aguas de Panamá* (Comisión de Reforma Agraria, República de Panamá, Panama City, Panama).
9. Bruijnzeel LA (2004) Hydrological functions of tropical forests: Not seeing the soil for the trees? *Agric Ecosyst Environ* 104(1):185–228.
10. Hawkins RH (1993) Asymptotic determination of curve numbers from data. *J Irrig Drain Eng* 119(2):334–345.
11. Hawkins R (1973) Improved prediction of storm runoff in mountain watershed. *J Irrig Drain Div* 99:519–523.
12. Calvo-Gobbeti LE, Ogden FL, Hendrickx JMH (2005) Infiltration in the Upper Rio Chagres basin, Panama: the soil conservation service "curve numbers". *The Rio Chagres, Panama: A Multidisciplinary Profile of a Tropical Watershed*, ed Harmon RS (Springer, Dordrecht, The Netherlands), pp 139–148.
13. Sharpley AN, Williams JR (1990) EPIC—Erosion/Productivity Impact Calculator: 1. Model documentation. *US Department of Agriculture Technical Bulletin* (US Department of Agriculture, Washington, DC).
14. Hawkins RH, Hjelmfelt AT, Jr., Zevenbergen AW (1985) Runoff probability, storm depth, and curve numbers. *J Irrig Drain Eng* 111(4):330–340.
15. Hawkins RH, Ward TJ, Woodward DE, Van Mullem JA (2009) *Curve Number Hydrology: State of the Practice* (American Society of Civil Engineers, Reston, VA).
16. USDA Natural Resources Conservation Service (2004) Hydrologic soil-cover complexes. *National Engineering Handbook, Part 630: Hydrology* [Natural Resources Conservation Service (NRCS), Washington, DC], Chap 9.
17. Neitsch SL, Arnold JG, Kiniry JR, Williams JR, King KW (2005) *Soil and Water Assessment Tool (SWAT): Theoretical Documentation, Version 2005* (Texas Water Resources Institute, College Station, TX).
18. Neilson RP, Marks D (1994) A global perspective of regional vegetation and hydrologic sensitivities from climatic change. *J Veg Sci* 5:715–730.
19. Scurlock JMO, Asner GP, Gower ST (2001) *Worldwide Historical Estimates and Bibliography of Leaf Area Index, 1932-2000* (Oak Ridge National Laboratory, Oak Ridge, TN).
20. Arnold JG, Allen PM, Bernhardt G (1993) A comprehensive surface-groundwater flow model. *J Hydrol (Amst)* 142:47–69.
21. Heckadon-Moreno S, Ibáñez R, Condit R (1999) *La Cuenca del Canal: Deforestación, Contaminación, y Urbanización* [*The Basin of the Canal: Deforestation, Pollution, and Urbanization*] (Smithsonian Tropical Research Institute, Balboa, Panama). Spanish.
22. Gibbs HK, Brown S, Niles JO, Foley JA (2007) Monitoring and estimating tropical forest carbon stocks: Making REDD a reality. *Environ Res Lett* 2:1–13.
23. Achard F, et al. (2002) Determination of deforestation rates of the world's humid tropical forests. *Science* 297(5583):999–1002.
24. Cairns MA, Brown S, Helmer EH, Baumgardner GA (1997) Root biomass allocation in the world's upland forest. *Oecologia* 111:1–11.
25. Houghton RA, Lawrence KT, Hackler JL, Brown S (2001) The spatial distribution of forest biomass in the Brazilian Amazon: A comparison of estimates. *Glob Change Biol* 7: 731–746.
26. Ramankutty N, et al. (2007) Challenges to estimating carbon emissions from tropical deforestation. *Glob Change Biol* 13:51–66.
27. Delaney M, Brown S, Lugo AE, Torres-Lezama A, Bello Quintero N (1998) The quantity and turnover of dead wood in permanent forest plots in six life zones of Venezuela. *Biotropica* 30:2–11.
28. Brown S, et al. (2000) Issues and challenges for forest-based carbon-offset projects: A case study of the Noel Kempff Climate Action Project in Bolivia. *Mitig Adapt Strategies Glob Change* 5:99–121.
29. Neumann-Cosel L, Zimmermann B, Hall JS, van Breugel M, Elsenbeer H (2011) Soil carbon dynamics under young tropical secondary forests on former pastures–A case study from Panama. *For Ecol Manage* 261(10):1625–1633.
30. Dale VH, Brown S, Calderon MO, Montoya AS, Martinez RE (2003) Estimating baseline carbon emissions for the eastern Panama Canal watershed. *Mitig Adapt Strategies Glob Change* 8:323–348.
31. Kraenzel M, Castillo A, Moore T, Potvin C (2003) Carbon storage of harvest-age teak (Tectona grandis) plantations, Panama. *For Ecol Manage* 173:213–225.
32. Winjum JK, Brown S, Schlamadinger B (1998) Forest harvests and wood products: Sources and sinks of atmospheric carbon dioxide. *For Sci* 44:272–284.
33. Autoridad del Canal de Panamá (ACP) (2006) *Plan Maestro del Canal de Panamá* [*Master Plan of the Panama Canal*] (Panama Canal Authority, Panama City, Panama). Spanish.
34. Hamilton K, Sjardin M, Marcello T, Xu G (2008) *Forging a Frontier: State of the Voluntary Carbon Markets 2008* (Ecosystem Marketplace, Washington, DC).
35. Campbell A, et al. (2008) *Carbon Emissions from Forest Loss in Protected Areas* (United Nations Environment Programme and World Conservation Monitoring Centre, Cambridge, UK).
36. Laurance WF (2007) A new initiative to use carbon trading for tropical forest conservation. *Biotropica* 39(1):20–24.
37. Neef T, Eichler L, Deecke I, Fehse J (2007) *Update on Markets for Forestry Offsets* [The Tropical Agricultural Research and Higher Education Center (CATIE), Turrialba, Costa Rica].
38. Autoridad del Canal de Panamá (ACP) (2003) *Recopilación y Presentación de Datos Socioeconómicos de la Región Occidental de la Cuenca del Canal de Panamá* [*Socioeconomic Data of the Western Region of the Panama Canal Basin*] (Panama Canal Authority, Panama City, Panama). Spanish.
39. González Murray RA, Guerra P, Ríos R, De León R (2009) *Comportamiento Productivo y Reproductivo del Ganado Bovino Criollo de Panamá Bajo Condiciones Mejoradas en la Estación Experimental de Gualaca* [*Productive and Reproductive Behavior of "Criollo" Cattle of Panama under Better Conditions at the Experimental Station of Gualaca*] [Instituto de Investigación Agropecuaria de Panamá (IDIAP), Panama City, Panama]. Spanish.
40. Salazar G, Salas N (2009) *Precios de la Madera en Costa Rica (Primer Semestre 2009)* [*Timber Prices in Costa Rica (First Semester 2009)*] (Oficina Nacional Forestal, Heredia, Costa Rica). Spanish.
41. Khatun K (2011) Reconciling timber provision with carbon sequestration opportunities in tropical forests of Central America. *Environ Sci Policy* 14:1091–1102.
42. Piotto D, Craven D, Montagnini F, Alice F (2010) Silvicultural and economic aspects of pure and mixed native tree species plantations on degraded pasturelands in humid Costa Rica. *New For* 39:369–385.
43. Aylward B (2002) *Strategic Framework. Report to the World Bank as Part of the Program for the Sustainable Management of the Rural Areas in the Panama Canal Watershed* (Aylward Private Consultancy, Falls Church, VA).

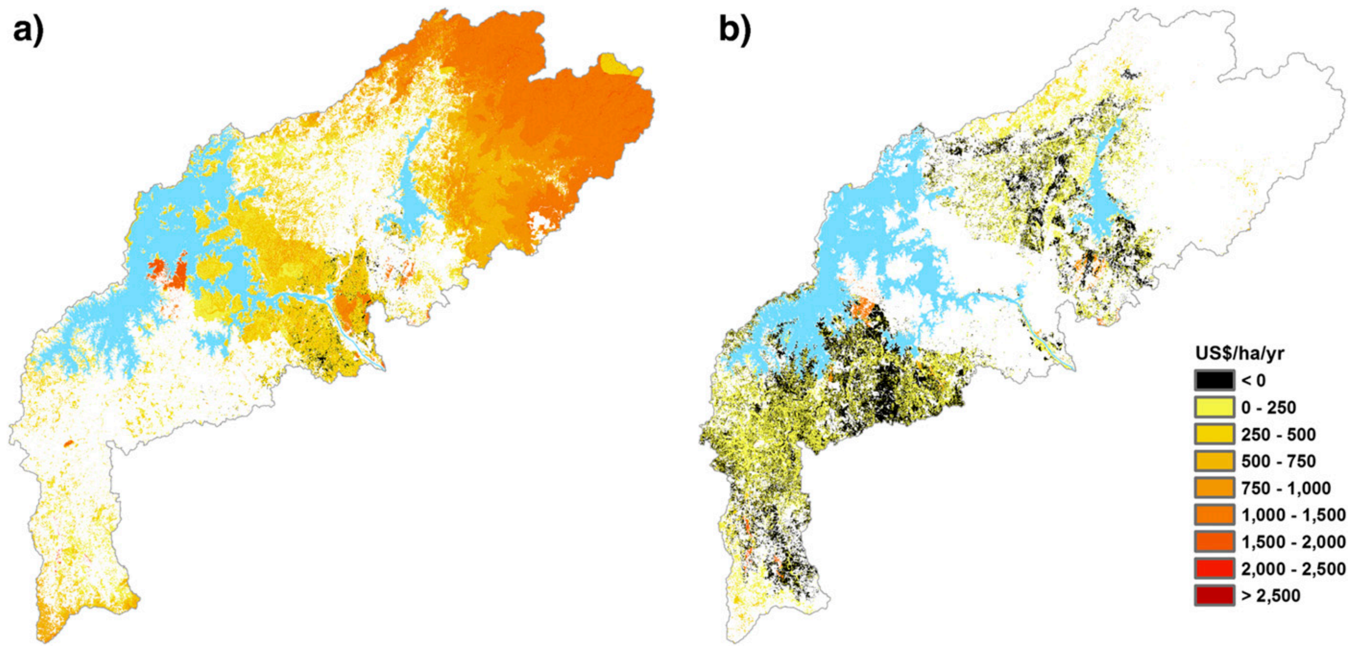

Fig. S1. Estimated steady-state annual average values for the bundle of dry-season flow regulation and carbon storage services generated by natural forest in the Panama Canal watershed. (*A*) Value of dry-season water flows and sequestered carbon generated by existing forest cover. (*B*) Value of dry-season water flows and sequestered carbon generated by conversion of grassland to "natural" forest.

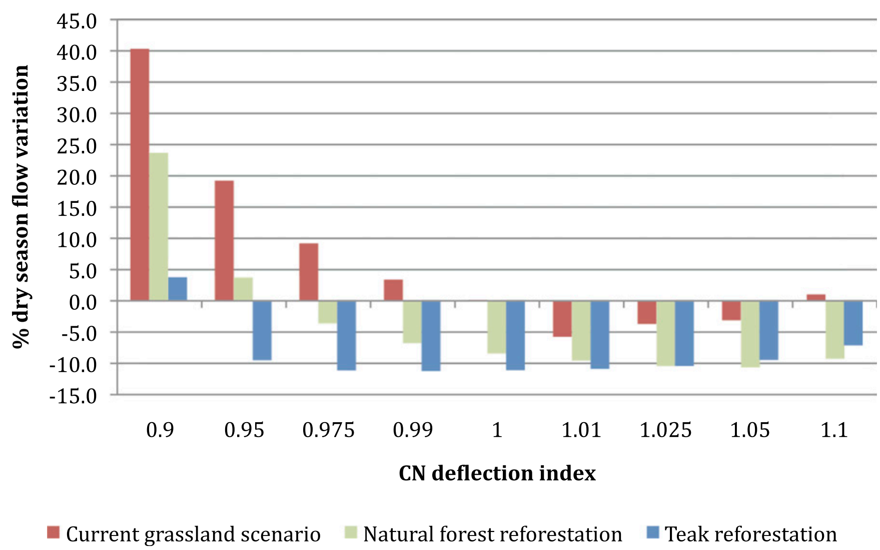

Fig. S2. Sensitivity analysis of dry-season flow to *CN* parameter values. Sensitivity analysis results have been obtained multiplying the *CN* value at each pixel (Fig. S6*C*) by the deflection index and then summing up the variation in hydrological flows across all pixels.

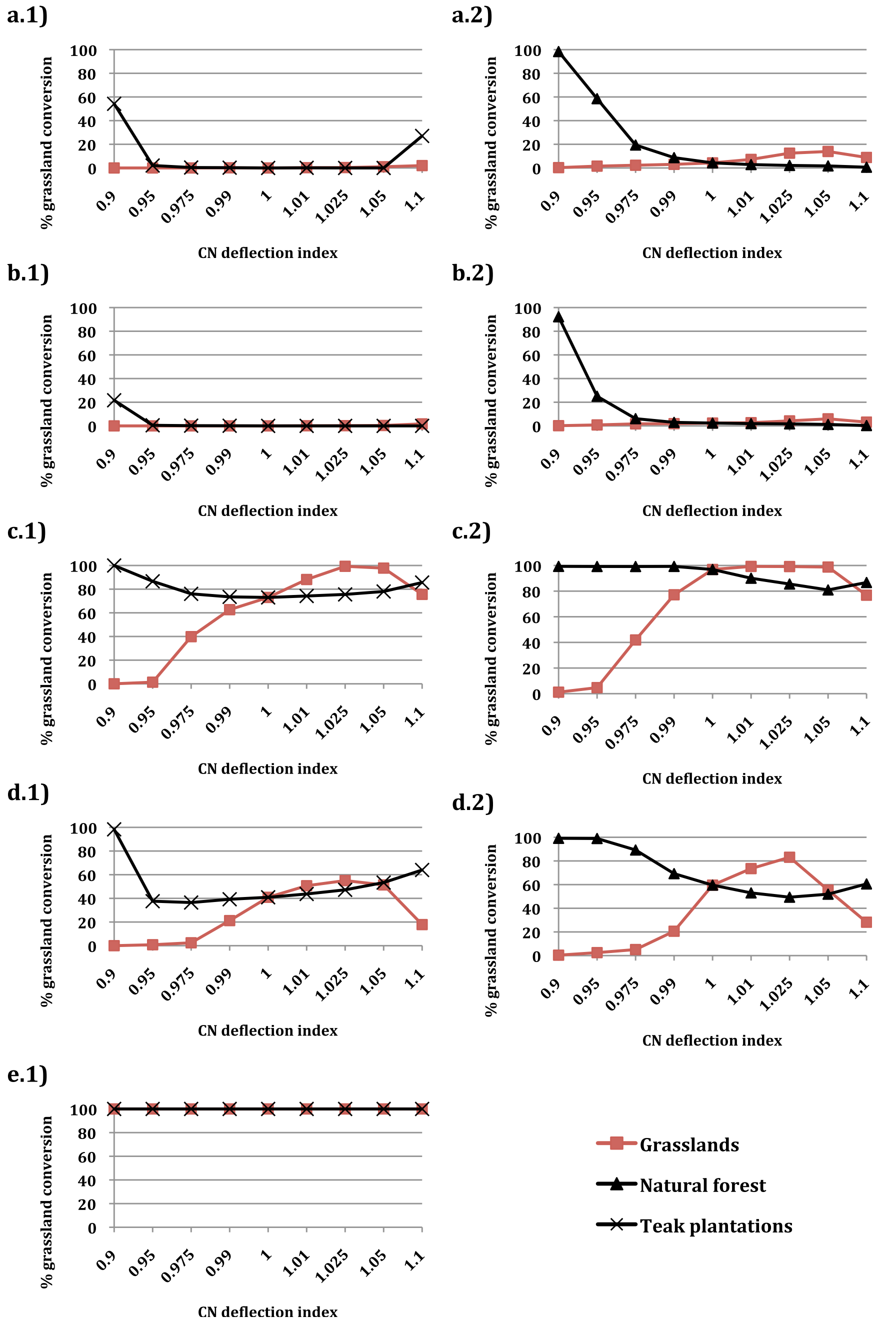

Fig. S3. Sensitivity analysis of grassland conversion to *CN* parameter values. (*A.1*–*E.1*) Grassland conversion to teak plantation for: (*A.1*) water regulation; (*B.1*) water regulation and livestock production; (*C.1*) water regulation and carbon sequestration; (*D.1*) water regulation, carbon sequestration, and livestock production; and (*E.1*) water regulation, carbon sequestration, livestock production, and timber. (*A.2*–*D.2*) Grassland conversion to natural forest for: (*A.2*) water regulation; (*B.2*) water regulation and livestock production; (*C.2*) water regulation and carbon sequestration; and (*D.2*) water regulation, carbon sequestration, and livestock production.

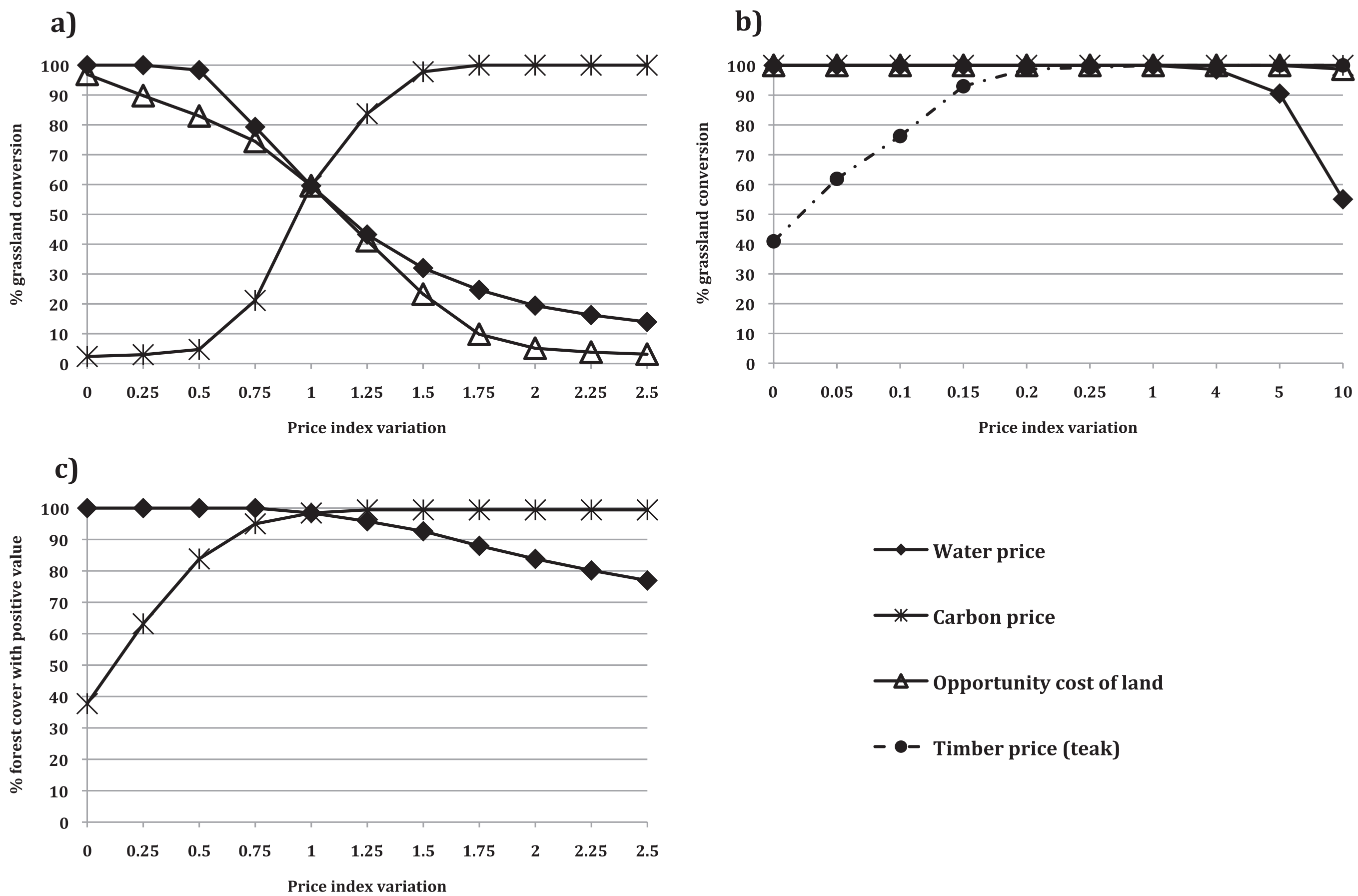

Fig. S4. Sensitivity analysis to price variations. (*A*) Sensitivity analysis of grassland conversion to natural forest. (*B*) Sensitivity analysis of grassland conversion to teak plantations. (*C*) Sensitivity analysis of current forest cover with positive value.

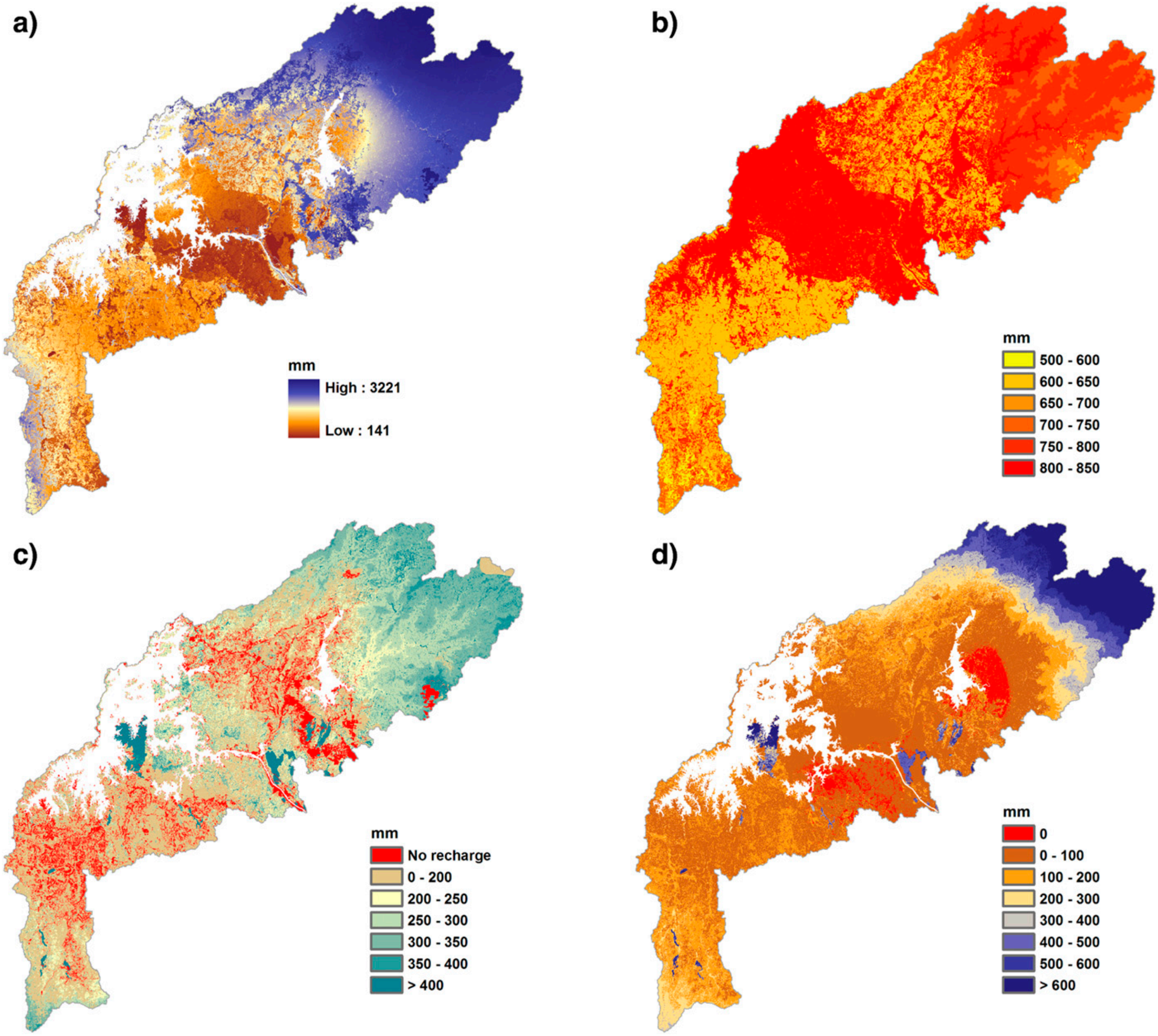

Fig. S5. Estimated spatial distribution of hydrological flows. (*A*) Predicted spatial distribution of wet-season runoff obtained from application of the SCS-Curve Number approach and using the spatially distributed *CN* value (Fig. S6*C*) as input in Eqs. **S1** and **S2**. (*B*) Wet-season actual evapotranspiration was obtained from monthly maps of potential evapotranspiration (PET) and the leaf area coefficient. (*C*) Predicted groundwater recharge was calculated using the water balance approach, overlaying the wet-season rainfall map with *A* and *B*. (*D*) Predicted spatial distribution of dry-season hydrological discharge calculated as the sum of surface runoff and groundwater flows. Sources: authors' calculations. Evapotranspiration data from geographic information system (GIS) maps of monthly PET were provided by ETESA.

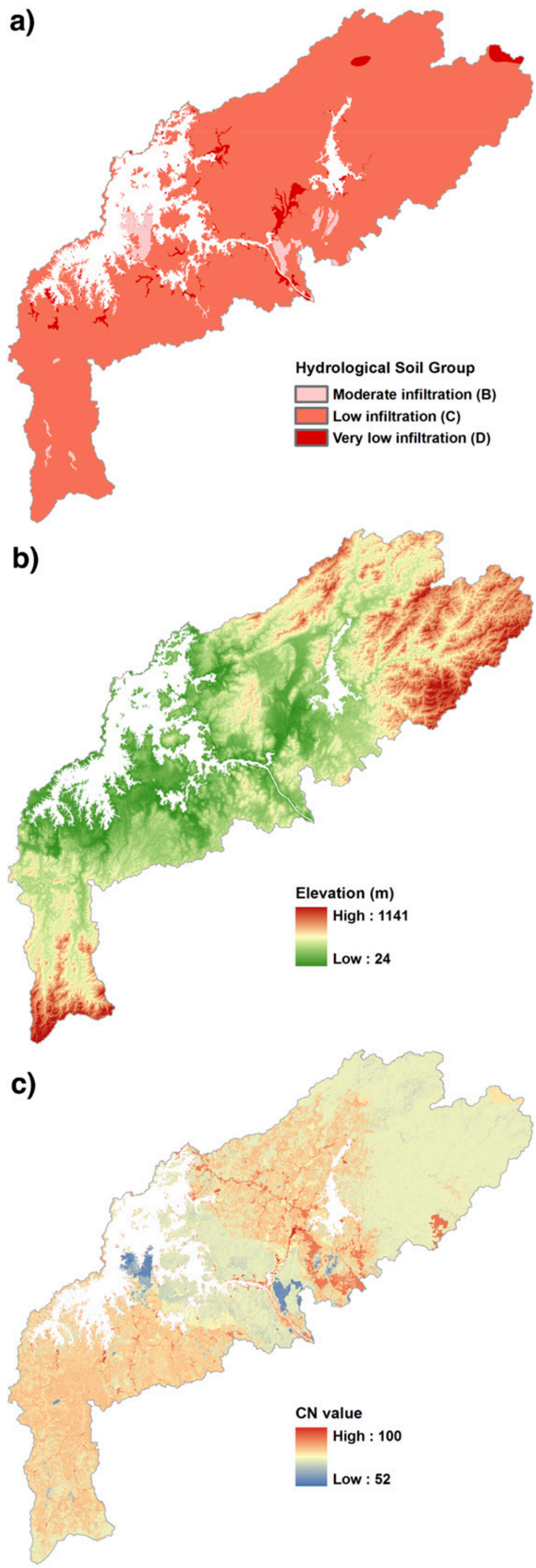

Fig. S6. Estimated spatial distribution of SCS-Curve Number across the Panama Canal watershed. (*A*) Spatial distribution of hydrological soil groups. (*B*) Digital elevation model. (*C*) Spatial distribution of slope-adjusted Curve Number indexes derived from *A* and *B* and Fig.1 and Table S4 and applying the Sharpley and Williams equation to adjust for slope. Sources: Authors' calculations. *A* was estimated from the Catapan soil characteristics map in ref. 1. Digital elevation model (30 × 30 m) was provided by the ACP. The Sharpley and Williams equation was obtained from ref. 2.

1. Catastro Rural de Tierras Y Aguas de Panamá (1970) Final Report on the Catastro Rural de Tierras y Aguas de Panamá (Comisión de Reforma Agraria, República de Panamá, Panama City, Panama).
2. Sharpley AN, Williams JR (1990) EPIC—Erosion/Productivity Impact Calculator: 1. Model documentation. US Department of Agriculture Technical Bulletin (US Department of Agriculture, Washington, DC).

Table S1. Estimated hydrological flows for gauged subbasins in the Panama Canal watershed: Wet-season runoff

Subbasin	Observed runoff volume, $m^3 \times 10^6$	Observed runoff depth, mm	Under-/overprediction at $\lambda = 0.2$, %	Under-/overprediction at $\lambda = 0.7$, %
Candelaria	373.72	2,599	9.3	−4.4
Los Canones	267.47	1,359	22.8	4.1
Ciento	181.31	1,589	28.3	9.4
Peluca	209.81	2,318	10.0	−4.3
Chico	860.77	2,125	15.2	−1.2
El Chorro	193.23	1,153	28.7	7.2

Source: authors' calculations. Observed flows from river gauge data are by the ACP.

Table S2. Estimated hydrological flows for gauged subbasins in the Panama Canal watershed: Dry-season flows

Subbasin	Observed total flow discharge, $m^3 \times 10^6$	Predicted potential baseflow, $m^3 \times 10^6$	Predicted net baseflow, $m^3 \times 10^6$	Predicted surface runoff, $m^3 \times 10^6$	Predicted total flow discharge, $m^3 \times 10^6$	Under-/overprediction of total flow, %
Candelaria	73.00	47.31	36.33	40.31	76.64	5.0
Los Canones	32.65	24.13	15.39	16.57	31.96	−2.1
Ciento	23.59	21.15	11.22	14.39	25.61	8.5
Peluca	35.91	24.26	17.35	19.93	37.28	3.8
Chico	195.65	127.30	87.05	100.75	187.80	−4.0
El Chorro	23.12	16.43	8.27	14.23	22.50	−2.7

Source: authors' calculations. Observed flows from river gauge data are by the ACP.

Table S3. Estimated hydrological flows for the two main subbasins of the Panama Canal watershed under different LULC scenarios

	Estimated water flows under current land use and land cover		Variation from current flows assuming all forest is converted to grassland		Variation from current flows assuming conversion of forest only in suitable slope, soil, and rainfall conditions	
Flow component	Gatun, $m^3 \times 10^6$	Madden, $m^3 \times 10^6$	Gatun, %	Madden, %	Gatun, %	Madden, %
Wet-season runoff	2,514	1,980	+12.3	+18.5	+1.8	+11.5
Groundwater recharge, wet season	278	269	−60.2	−79.9	−10.9	−51.0
Dry-season evapotranspiration	900	482	−10.0	−20.2	−1.1	−12.0
Soil moisture deficit, dry season	170	112	−95.4	−99.6	−10.4	−32.5
Baseflow, dry season	108	157	−4.7	−65.8	−11.8	−64.4
Dry-season runoff	96	170	+32.9	+51.5	+5.2	+41.9
Dry-season total flow	204	327	+13.0	−4.7	−3.8	−9.0

Source: authors' calculations.

Table S4. Curve numbers table for the Panama Canal basin

Land cover type	CN(B)	CN(C)	CN(D)
Water bodies	100	100	100
Bare land	86	91	93
Residential areas and roads	85	90	92
Agriculture	75	83	86
Grassland	70	80	84
Shrubland vegetation	66	77	83
Forest plantation	60	73	79
Natural forest, primary and secondary	52	69	75

Source: authors' calculations of CN values for forest. CN values for other LULCs were taken from the literature.